White Noise from Dark Matter: 21 cm Observations of Early Baryon Collapse

Kathryn M. Zurek
Department of Physics, University of Wisconsin, Madison, WI 53706

Craig J. Hogan
Departments of Physics and Astronomy, University of Washington, Seattle, WA 98195

arXiv:astro-ph/0703624v1 26 Mar 2007

In concordance cosmology, dark matter density perturbations generated by inflation lead to nonlinear, virialized minihalos, into which baryons collapse at redshift $z \sim 20$. We survey here novel baryon evolution produced by a modification of the power spectrum from white noise density perturbations at scales below $k \sim 10h$ Mpc^{-1} (the smallest scales currently measured with the Lyman-α forest). Exotic dark matter dynamics, such as would arise from scalar dark matter with a late phase transition (similar to an axion, but with lower mass), create such an amplification of small scale power. The dark matter produced in such a phase transition collapses into minihalos, with a size given by the dark matter mass within the horizon at the phase transition. If the mass of the initial minihalos is larger than $\sim 10^{-3} M_\odot$, the modified power spectrum is found to cause widespread baryon collapse earlier than standard ΛCDM, leading to earlier gas heating. It also results in higher spin temperature of the baryons in the 21 cm line relative to ΛCDM at redshifts $z > 20$ if the mass of the minihalo is larger than $1M_\odot$. It is estimated that experiments probing 21 cm radiation at high redshift will contribute a significant constraint on dark matter models of this type for initial minihalos larger than $\sim 10M_\odot$. Early experiments reaching to $z \approx 15$ will constrain minihalos down to $\sim 10^3 M_\odot$.

I. INTRODUCTION

The concordance cosmological model (Cold Dark Matter with cosmological constant, ΛCDM) explains cosmological structural data over four orders of magnitude in linear scale. Cosmic background anisotropy [1], galaxy surveys [2, 3], and Lyman-α forest statistics [4] all accord with a model of non-interacting, non-relativistic matter, whose density perturbations are seeded by inflation and are nearly scale free. As far as the present cosmological data on these scales are concerned, the particle properties of the dark matter are irrelevant, provided that the dark matter candidate is sufficiently cold and collisionless; the effects of the dark matter are set not by the internal properties of the dark matter itself (e.g. mass and interactions), but by the perturbations imprinted at very early times through inflation [5]. The modifications to the inflationary perturbation spectrum by the leading dark matter candidates, the Weakly Interacting Massive Particle (WIMP) and the axion, are so small that their effect on structure formation will be very difficult to observe. For the WIMP, these modifications arise only at earth mass scales [6], while for the axion, the modifications occur at an even smaller scale of $10^{-12} M_\odot$ [7].

This idealized cold and collisionless model of dark matter, however, may not apply on small scales. The physics of dark matter may be consistent with all current data but lead to new and measurable effects on smaller scales, yielding signatures which are unique to each candidate. For example, there has been much work done to explain discrepancies between the predictions of ΛCDM and the observed number of dwarf satellites and their central densities by modifying the small scale dynamics of dark matter. These include adding dark matter interactions [8] or annihilations [9] with cross-sections roughly the size of hadronic cross-sections. Other models modify the small scale power (on Lyα scales of $k \simeq 10h$/Mpc) by changing the free-streaming scale through late warming of the dark matter, as in certain supersymmetric models with a late decay of the next-to-lightest supersymmetric partner [10, 11], or through primordially warm keV mass sterile neutrino dark matter [12, 13, 14].

Here we are interested in a different generic modification to small scale behavior introduced by new dark matter physics: that associated with added fluctuation power on small scales, in particular additional power with a white noise spectrum. As discussed below, this added noise is a generic byproduct of the process that makes scalar dark matter during a phase transition. Since the spectrum is known the effects are characterized by one number, the amplitude of the added noise.

Without loss of generality for the scales considered here, we choose to characterize this extra fluctuation power as shot noise arising from discrete primordial lumps of dark matter, such as black holes or minihalos. When the universe becomes matter dominated they give rise to an additional power spectrum:

$$P_{wn} = \frac{1}{n_H} = \frac{M_H}{\rho_{DM}}, \tag{1}$$

where M_H denotes the mass of the lumps (be they halos or holes). Note that such a power spectrum is wavenumber independent so that at sufficiently large k it dominates over the inflationary spectrum, which drops as k^{-3}.

Primordial black hole dark matter is itself highly constrained by astrophysical effects other than their effect on the power spectrum; in particular, strong gravitational lensing experiments now rule out primordial black holes with $M_H \gtrsim 10^{-7} M_\odot$ (with the possible exception of a small window around $100M_\odot$). On the other hand for

scalar dark matter the primordial minihalos are not particularly compact, but have a density determined by the first self-gravitating collapse, at around the epoch of matter domination; thus the dark matter minihalos are not always of negligible size but instead are gravitationally bound diffuse systems, hence the name "minihalos". In this case the lensing properties of the minihalos (termed "scalar miniclusters" as studied in [15]) depend on the distance, mass and mass profile; current bounds from lensing, and from the Lyα forest power spectrum measurements, allow M_H as large as $\approx 4 \times 10^3 M_\odot$ [15, 16].

Here we survey the effects of primordial white noise on early baryon evolution, such as early gas collapse, heating, and star formation, and their possibly observable effects in forthcoming experiments [17, 18] designed to directly measure signals from hydrogen hyperfine transitions at the epoch of cosmic reionization and higher redshifts. The standard ΛCDM models of these events [19, 20, 21] show a significant range of possible behavior for $z < 20$ after stars begin to form, since observables depend significantly on the output of stellar populations. We do not present such detailed models here, but estimate the range of M_H for which various departures from standard cosmology are expected to be appreciable and observable at higher redshifts before stellar activity becomes significant in ΛCDM.

These are our main conclusions about the effects of the added white noise, depending on the mass M_H of the initial seed minihalos (which in turn depends on the scalar particle mass):

- Minihalos with M_H below about $10^{-3} M_\odot$ cause essentially no new effects. They create halos whose virial temperature is always too low to accrete baryons.

- Minihalos in the range $10^{-3} M_\odot < M_H < 1 M_\odot$ add to inflationary power significantly, enough to influence baryon collapse at redshift $z < 30$, but the added effects may be difficult to distinguish observationally from moderately rare ($\approx 2\sigma$) inflationary perturbations.

- Minihalos as small as $M_H \approx 1 M_\odot$ create halos whose virial temperature is high enough to accrete and heat baryons at $z \gtrsim 30$, well before these effects occur widely in ΛCDM (at $z < 20$). This modifies the standard predictions for quantities affecting potential observables, such as the spin temperature of the gas in the range $20 < z < 50$, even though the spatial distribution of gas on larger scales is little affected. The departures have clear signatures: the kinetic and spin temperatures of the gas are higher than in standard cosmology and begin activity at much higher redshift. On the other hand the departure of spin temperature is rather small at $z \lesssim 50$, making detection difficult.

- Minihalos above $M_H \approx 10 M_\odot$ create halos whose virial temperature is high enough for 3σ fluctuations to result in molecular and atomic cooling at $z > 30$, allowing baryons to not only collapse, but also radiate, become self-gravitating and form stars much earlier than ΛCDM (which predicts the first stars at $z < 20$). In this regime, experiments reaching beyond $z \approx 20$ should see significant differences from ΛCDM predictions. Indeed, for lumps at the current limit $M_H \approx 10^3 M_\odot$, collapse and star formation are expected already at the epoch of recombination. Star formation can have observable effects via infrared emission and enrichment. In addition, the spin temperature perturbation is many times larger than the standard prediction at redshift $z > 20$, and appears in emission rather than absorption.

We conclude that the future generations of high redshift experiments will likely provide new constraints on dark matter behavior, and may constrain initial minihalo mass as small as $M_H \approx 10 M_\odot$.

II. SCALAR DARK MATTER AND EXTRA WHITE NOISE POWER

Generically, any second order phase transition in the early universe, where a scalar field of very low mass evolves from fixed vev to oscillation about the potential minimum, generates density perturbations on the scale which is the horizon size at the phase transition, $d_H(T_{trans})$. The density fluctuations which arise from such a phase transition have two sources: classical or quantum fluctuations of the field. Consider a complex scalar field, $\phi = re^{ia/f}$; classical fluctuations come from the angular mode, a, and quantum fluctuations from the radial mode, r.

The classical fluctuations arise from spatial variations in the vev of a on scales larger than the horizon; on smaller scales, spatial gradients will align the field locally (the Kibble mechanism). When $H \sim m_a$, the field begins to oscillate around the true minimum at $\langle a \rangle = 0$, and dark matter will appear with density $\rho = \frac{1}{2} m_a^2 \langle a \rangle_i^2$. Since $\langle a \rangle$ has spatial fluctuations between $-\pi$ and π, the local dark matter density will have $O(1)$ density perturbations on the scale which is the horizon size at the time of the phase transition, $d_H(T_{trans})$. The QCD axion, for example, is marked by such fluctuations when the Peccei-Quinn symmetry breaks after inflation; the resulting structures, axion miniclusters, have been studied extensively in [15, 22, 23]. (Standard axion miniclusters have masses $M_h \sim 10^{-12} M_\odot$, determined by the mass of axions within the horizon at 1 GeV when the axion mass becomes large enough to start oscillations and dark matter formation.)

The second means to generate density fluctuations, through quantum fluctuations, requires only slightly more explanation. The size of the quantum fluctuations in the radial mode is set by its mass: $\langle \delta r \rangle \sim m_r$. These fluctuations in $\langle r \rangle$ lead to fluctuations in the time (or,

equivalently, the temperature) of the phase transition: $\delta t_{trans} \sim \langle \delta r \rangle / \langle \dot{r} \rangle$, where $\langle \dot{r} \rangle \sim m_r \langle r \rangle$ is the evolution of the background field, so that $\delta t_{trans} \sim 1/m_r$. The last observation is that the density fluctuations are proportional to the fluctuations in phase transition time (or equivalently, temperature)

$$\frac{\delta \rho}{\rho} = 3\frac{\delta T}{T} \sim H \delta t_{trans} \tag{2}$$

Since $\delta t_{trans} \sim 1/m_r$, $\delta\rho/\rho \sim H/m_r$. For a phase transition occurring just as the particle mass enters the horizon, density fluctuations will again be $O(1)$. The size of the density fluctuations can be suppressed if some finite temperature effects prevent the phase transition from occurring promptly, and instead $H/m_r < 1$.

We have shown that the density fluctuations on the scale $d_H(T_{trans})$ are non-linear. On smaller scales, density perturbations are damped since spatial gradients are able to align the field locally on a light-crossing timescale. On larger scales, the density perturbations are simply white noise, so that the total power spectrum is

$$P = \frac{M_H}{\rho_{DM}} e^{-(k d_H)^2/2}. \tag{3}$$

where M_H is the dark matter mass contained in $d_H(T_{trans})$. Note again that since this power spectrum is k independent up to the cut-off scale at d_H, the white noise spectrum will be insignificant at smaller k where the inflationary perturbations are most important, but may dominate the power spectrum at smaller scales where the inflationary spectrum scales as k^{-3}. A $10^3 M_\odot$ mass minihalo corresponds to a phase transition at 0.1 GeV or a 10^{-12} eV mass scalar.

The white noise power spectrum of eqn. 3 gives rise to novel, qualitatively different structure formation in the matter dominated era. Due to the large density fluctuations on small scales, virialization occurs much earlier, generally as early as T_{eq}. If the virialized potentials are deep enough, baryons begin to collapse onto the objects very early, altering the temperature and density of the gas; if further energy loss from cooling is efficient, the baryons can then cool to form stars.

III. STRUCTURE FORMATION WITH WHITE NOISE POWER SPECTRUM

In ΛCDM structure formation, all density perturbations are initially linear. After matter-radiation equality, they grow linearly with scale factor until the perturbations become $O(1)$. Using the Press-Schechter analytic approach to structure formation, the small scale objects are incorporated into larger objects hierarchically as the perturbations on larger scales themselves become non-linear. The first objects are typically formed at redshifts $z \sim 20$.

With the addition of white noise perturbations, we have a very different scenario. The initial power spectrum is characterized by non-linear dark matter fluctuations on the scale $d_H(T_{trans})$. On larger scales,the perturbations decrease with wavenumber as $k^{3/2}$. On scales where the perturbation is initially non-linear, structure is immediately formed at matter-radiation equality. On larger scales, the fluctuations grow linearly with redshift until they too become non-linear and collapse. This is written as a fractional rms variation in density on a certain mass scale,

$$\sigma(M, z) = \sigma(M)_i \frac{1 + z_{eq}}{1 + z} \tag{4}$$

where the variance is

$$\sigma^2(M, z = 0) = \int \frac{dk}{2\pi^2} P(k) \left[\frac{3 j_1(kR)}{kR} \right]^2, \tag{5}$$

$M = 4\pi\rho_m R^3/3$ and $j_1(x) = (\sin x - x \cos x)/x^2$ is a particular choice of window function for variance of mass within spheres. Using the white noise power spectrum, the density fluctuations can be approximated as

$$\sigma(M, z) \approx \sigma(M_H)_i \left(\frac{M}{M_H} \right)^{1/2} \frac{1 + z_{eq}}{1 + z} \tag{6}$$

where σ_i is a number of order unity set by the details of the phase transition and the form of the cutoff chosen for the white noise power spectrum. The initial power spectrum and density perturbations, σ_i are shown in figs. 1 and 2. Using the Press-Schechter approach, we expect an object of mass M to collapse and virialize during the matter-dominated era at a redshift z when $\sigma(M, z) \simeq 1.69$. In fig. 3, we show the masses of typical collapsing halos both in ΛCDM (dotted lines corresponding to 1 and 2σ fluctuations) and with added white noise (solid lines corresponding to seed masses $M_H = 10^{-6} M_\odot$, $10^{-3} M_\odot$, $1 M_\odot$, $10^3 M_\odot$). In this last scenario, significant structure formation begins as early as z_{eq}. The departures from ΛCDM become even more noticeable at higher redshifts, as shown in fig. 4. We can see that at high redshifts, more massive halos virialize much earlier with added white noise power

When the halo virial temperature of the collapsing halos rises above the temperature of the baryons, the baryons begin to accrete. The virial temperature for neutral primordial gas can be expressed in terms of the mass of the collapsing halo [19],

$$T_{vir} \approx 4 \times 10^4 \left(\frac{M}{10^8 h^{-1} M_\odot} \right)^{2/3} \left(\frac{\Omega_m}{\Omega_m^z} \right)^{1/3} \left(\frac{1 + z}{10} \right) \mathrm{K} \tag{7}$$

where $\Omega_m^z = \Omega_m (1+z)^3 / (\Omega_r (1+z)^4 + \Omega_m (1+z)^3 + \Omega_\Lambda)$. The virial temperature of typical collapsing halos as a function of redshift is shown in figs. 5 and 6, the analogs of figs. 3 and 4. Because of the higher virial temperature associated with collapsing halos from the amplified power

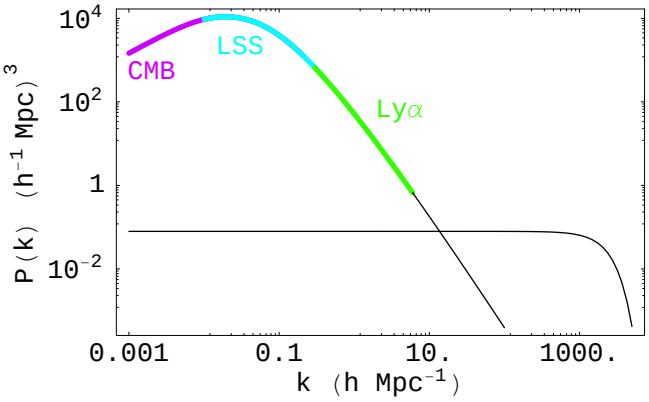

FIG. 1: Inflationary power spectrum and white noise power spectrum with $M_H = 10^3 M_\odot$. CMB, LSS and Lyα indicate the regions where the Cosmic Microwave Background, Large Scale Structure, and Lyα forest measurements constrain the power spectrum.

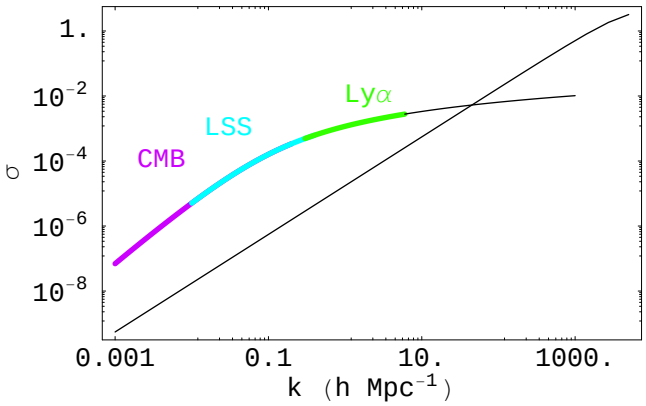

FIG. 2: Variance of inflationary perturbations and white noise power spectrum with $M_H = 10^3 M_\odot$. CMB, LSS and Lyα indicate the regions where the Cosmic Microwave Background, Large Scale Structure, and Lyα forest measurements constrain the power spectrum. The added variance at small scales produces early baryon collapse and observable effects at high redshift that would have escaped detection by the other techniques.

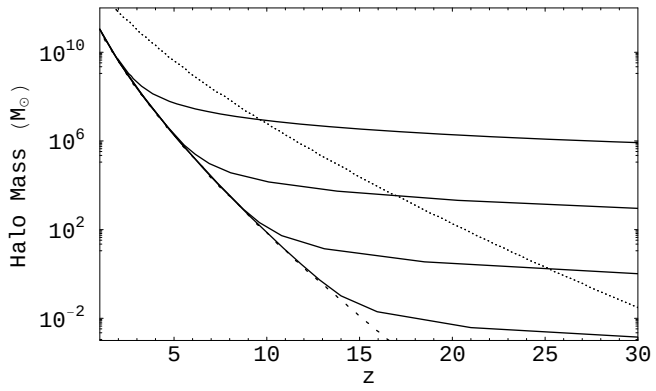

FIG. 3: Masses of typical collapsing halos as a function of redshift. The dotted lines correspond to 1 and 2σ fluctuations from an inflationary power spectrum. The solid lines show the deviation from ΛCDM for the addition of white noise power with seed masses $M_H = 10^{-6} M_\odot,\ 10^{-3} M_\odot,\ 1 M_\odot,\ 10^3 M_\odot$.

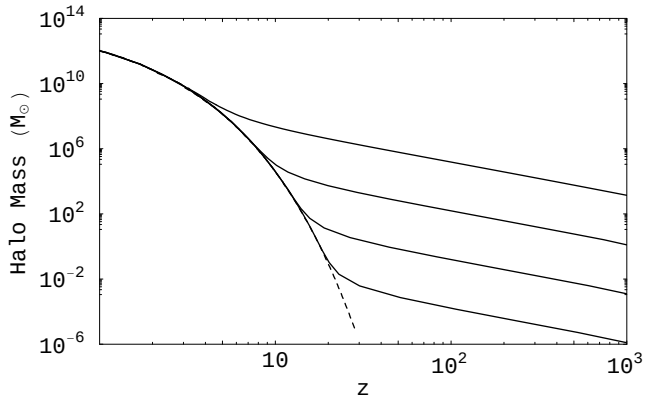

FIG. 4: Same as the previous figure, but extending to higher redshift. The figure shows the larger deviations from ΛCDM at high redshifts.

spectrum on small scales, baryons may collapse into halos at much higher redshifts. The heating may be sufficient to start early star formation and reionization as well.

When the baryons have collapsed into the halos, they are then heated via shocks and adiabatic compression to the virial temperature of the halo. If there is no further energy loss from cooling, the baryons then stabilize hydrostatically with gas pressure gradients balancing the gravitational attraction of the combined halo and baryon mass. On the other hand if cooling is possible, the energy loss allows further collapse; eventually the baryons become self gravitating and the collapse becomes unstable until the formation of stars provides heating to counteract the effect of cooling.

At $z \gtrsim 200$, Compton scattering typically couples the baryons to the CMB photons, and uncollapsed baryons cool as $(1+z)^{-1}$. When they decouple, uncollapsed baryons cool adiabatically, according to $(1+z)^{-2}$. When $z \gtrsim 200$ and baryons have begun accreting onto the halos, radiative loss occurs through Compton cooling; at any redshift, once the virial temperature reaches above 10^3 K and 10^4 K, molecular hydrogen and atomic cooling can occur, respectively. Dashed lines have been added to figs. 6 and 5 for the background baryon temperature, and the temperatures at which CMB, molecular, and atomic cooling become efficient. When the virial temperature rises above these lines, widespread efficient star formation can occur.

These figures illustrate a few basic behavior thresholds. For M_H less than about $10^{-3} M_\odot$, white noise creates early-collapsing halos but these are below the baryon temperature so they cause only small amplitude perturbations in the gas. There is no time at which baryon collapse occurs much differently from standard dark matter. For $M_H \approx 1 M_\odot$, baryons collapse commonly at $z \approx 50$,

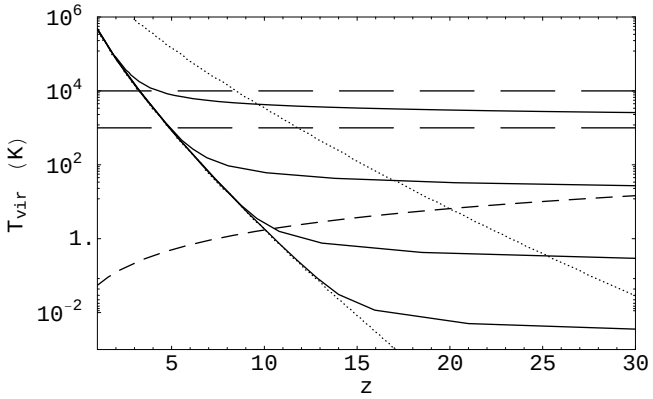

FIG. 5: Virial temperature (in Kelvin) of typical collapsing objects, as a function of redshift. The dotted lines correspond to 1 and 2σ fluctuations from an inflationary power spectrum. The solid lines show the deviation from ΛCDM for the addition of white noise power with seed masses $M_H = 10^{-6}M_\odot$, $10^{-3}M_\odot$, $1M_\odot$, $10^3M_\odot$. When the virial temperature rises above the temperature of the unperturbed baryons (shown by short dashed line), the baryons collapse onto the dark matter structure, leading to very early clumping and heating. In addition, when the virial temperature is above 10^3 and 10^4 Kelvin (shown by long dashed lines), molecular and atomic cooling, respectively, may proceed, and the clumped baryons begin to form stars. Seeds above about $1M_\odot$ cause widespread nonlinear gas collapse at $z > 30$, significantly earlier than ΛCDM; those above $10^2M_\odot$ produce widespread cooling and star formation at high redshift $z > 30$; those above about $10M_\odot$ do so for 3σ fluctuations.

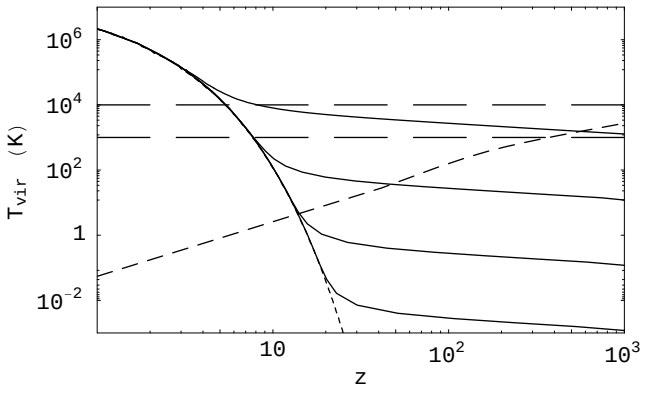

FIG. 6: Same as the previous figure, but extending to higher redshift. The figure shows the larger deviations from ΛCDM at high redshifts

much earlier than usual, and they are heated by adiabatic compression and shock heating, to temperatures well above the standard model, even without the action of stars. Presumably a closer study would reveal that these models also form some stars, in rare high density peaks able to cool, and that this also happens much earlier than usual. For $M_H > 10^2M_\odot$ it becomes widespread (at the 1σ level) to form stars at $z > 30$ above the molecular cooling threshold. Finally, for $M_H \approx 10^3M_\odot$, the halos accrete gas already at recombination, at a temperature where cooling is efficient, so star formation is widespread and the gas temperature well above the radiation temperature at all redshifts.

IV. SPIN TEMPERATURE HEATING AND 21 CM TOMOGRAPHY

We do not consider in detail heating and ionization from these first very early stars, or the Wouthuysen-Field effect by which transitions induced by stellar Lyα photons help to couple the spin temperature to the kinetic temperature of the gas. Instead we aim to estimate simply the amount of white noise power needed to make an observable departure from the behavior of standard ΛCDM. It is a reasonable first approximation, even in the presence of stellar heating, to assume that the typical temperature of the bulk of diffuse gas is about the virial temperature of the dark matter halos; much hotter gas would be expelled and cool by expansion, whereas much colder gas would collapse and form stars, until the stellar feedback is sufficient to heat the gas and halt collapse. We know from surveys of baryons today (which are still mostly in diffuse hot ionized gas) that most of the gas did not form stars in the end so such feedback must have operated rather efficiently.

A relatively clear signature of these effects may appear in 21 cm transitions in gas at high redshifts. The observable effects on antenna temperature fluctuations scale with the spin temperature of the bulk of relatively diffuse gas, which in our scenario is significantly modified by the presence of the white noise. To estimate the redshift and magnitude of departures from the standard model we adopt here a simplified model of gas density, kinetic and spin temperatures, adequate for identifying the thresholds of significant observable departures from ΛCDM. A more complete account of the relevant physics, and more detailed models for ΛCDM, can be found in [19, 20].

The strength of the transition is characterized by the spin temperature, which relates the relative populations of the ground and excited states of the 21 cm transition through $n_1/n_0 = 3e^{-T_*/T_S}$, where $T_* = 0.068$ K. This spin temperature is controlled by a balance of radiative and collisional transitions, so that the spin temperature can be related to the background radiation and kinetic temperatures, T_γ and T_K:

$$T_S = \frac{T_\gamma + yT_K}{1+y}. \tag{8}$$

y depends on the radiative and collisional Einstein coefficients, so that $y \propto n_H$, the number density of hydrogen. It is computed from the tables in [20]. T_γ is the temperature of the radiation that is absorbed or stimulates 21 cm emission; this is dominated by CMB photons, $T_\gamma = T_{CMB}$. If $T_S > T_{CMB}$, the resulting excess radiation brightness temperature through the cloud is given

by

$$T_b = T_S(1 - e^{-\tau}) \simeq \tau T_S, \tag{9}$$

where τ is the optical depth:

$$\tau = \frac{3A_{10}n_H}{16\nu_0^2 T_S H(z)}. \tag{10}$$

Here $A_{10} = 2.85 \times 10^{-15}$ s^{-1} is the spontaneous emission coefficient for the transition, and $\nu_0 = 1420.4$ MHz is the rest frame transition frequency. Notice that when $T_S > T_{CMB}$ the transition is seen in emission, and the brightness temperature is independent of the spin temperature. If, on the other hand, $T_S < T_{CMB}$, then the transition is seen in absorption, with brightness temperature

$$\begin{aligned} T_b &= T_{CMB}e^{\tau} + T_S(1 - e^{-\tau}) \\ &\simeq (T_S - T_{CMB})\tau. \end{aligned} \tag{11}$$

In standard CDM, the baryons do not collapse onto nonlinear dark matter structures until $z \lesssim 20$, so that at higher redshift their temperature evolves uniformly with the background. At $z \gtrsim 200$, Compton scattering couples the baryons to the photons, so that the temperature of the baryons is the same as the CMB temperature: $T_K \simeq T_{CMB}$. The number density of hydrogen is high enough that $y \propto n_H \gg 1$ and $T_S \simeq T_K$. Once the photons and baryons decouple, the uncollapsed baryons cool adiabatically, $T_K \sim (1+z)^2$. The spin temperature continues to track T_K until the number density of hydrogen becomes small enough that $y \lesssim 1$. T_S then again tracks T_{CMB}. As a result, at some intermediate redshifts, the spin temperate interpolates between the kinetic temperature and the photon temperature, and $T_S < T_{CMB}$. We show this scenario in fig. 7. One may also in principle see density and temperature inhomogeneities in the intervening hydrogen through absorption of CMB photons in the 21 cm line [24].

The addition of the white noise power to the standard ΛCDM fluctuations from inflation leads to larger dark matter density fluctuations on small scales. As a result, dark matter structures form earlier than in standard ΛCDM. The virial temperature of early-formed dark matter structures is continually rising with decreasing redshift (see fig. 6). As was shown in fig. 6, when that virial temperature rises above the baryon temperature, the baryons clump onto the just-formed dark matter structures. The virial temperature of these dark matter structures is higher than in standard ΛCDM, so that the kinetic temperature of the gas collapsing onto the virialized dark matter is also higher than in standard ΛCDM. As a result, the spin temperature of the gas tracks the hotter baryons. Of course, in the limit of sufficiently small white noise power, the spin temperature should reduce to the CDM result. This situation is shown in fig. 8, with a zoom in at lower temperatures in fig. 9. For sufficiently high M_H the spin temperature may actually be

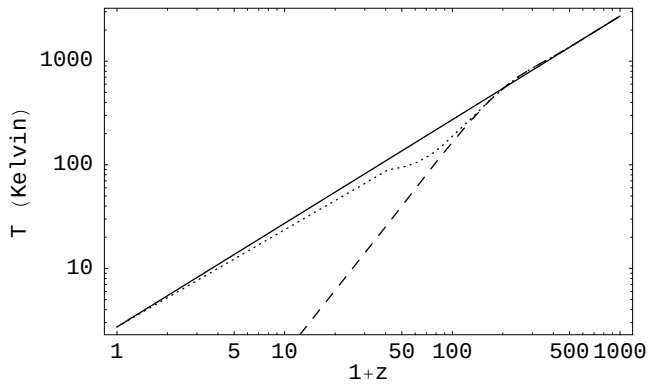

FIG. 7: Evolution of spin temperature (short dashed line) of uncollapsed baryons in (simplified) standard CDM due to coupling with CMB photons. At intermediate redshifts, the spin temperature interpolates between the kinetic temperature of the baryons, T_K (long dashed), and the CMB temperature T_{CMB} (solid). As a result, the 21-cm line is seen in absorption, $T_S < T_{CMB}$, at those redshifts.

greater than the CMB photons when it would be less in ΛCDM.

Thus for large enough amplitude white noise power the hyperfine transition is seen in emission, rather than absorption (that is, $T_S > T_{CMB}$). For $M_H = 10^3 M_\odot$, the gas is *always* seen in emission. Even with (typical models of) heating from star formation included, this behavior *never* occurs at intermediate or high redshifts ($z \gtrsim 15$) with standard CDM. In this high power case, the 21cm signals are also larger, by a large factor, than those predicted in standard models, especially at higher redshift. Thus, dark matter models in this range should be significantly constrained by tomographic experiments that reach the ΛCDM sensitivity level even at $z \approx 15$.

We note that 21cm tomographic experiments measure differential anisotropy, and are designed to seek particular signatures of structures in frequency and angle. The basic design of these experiments does not distinguish between emission and absorption in the linear regime. The main signatures of white noise then arise from having departure of $|T_S - T_\gamma|$ from ΛCDM, particularly from effects of inhomogeneous (virial or stellar) heating at redshifts $z > 20$ where ΛCDM makes clean predictions, because no nonlinear structures or stars have yet formed. In addition, there are also experiments under development to test the specific spectral signature of 21 cm absorption and emission; these would be able to detect more directly the radical departure of these models from ΛCDM predictions for spin temperature.

In the case of small seed structures (corresponding to smaller amplitude white noise), heating by halos alone may not be sufficient to raise the spin temperature above T_{CMB}, but, as can be seen from fig. 8, the spin temperature is nevertheless higher than standard CDM. As the radiation from the first stars may serve to further raise the kinetic temperature, and hence the spin temperature,

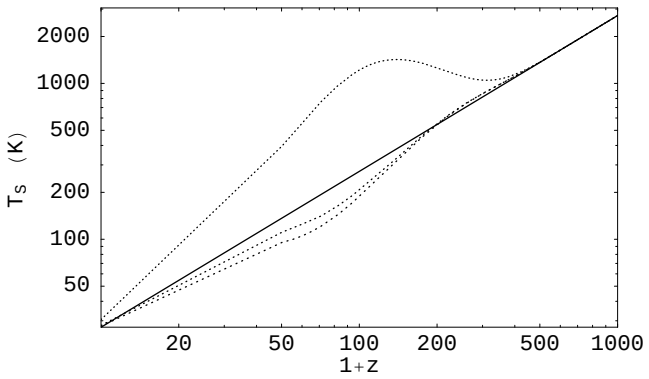

FIG. 8: Spin temperatures of newly formed objects, for seed white noise power (from top to bottom, $M_H = 10^{-6}M_\odot,\ 10^{-3}M_\odot,\ 1M_\odot,\ 10^3M_\odot$). The 10^{-3} and $10^{-6}M_\odot$ curves are indistinguishable from each other and the predictions of CDM (the dashed line in fig. 7). For comparison to the background CMB temperature, T_{CMB} is the solid line. The coupling of all kinetic temperatures at $z \gtrsim 200$ to the CMB temperature is the result of coupling of photons and baryons at high redshift.

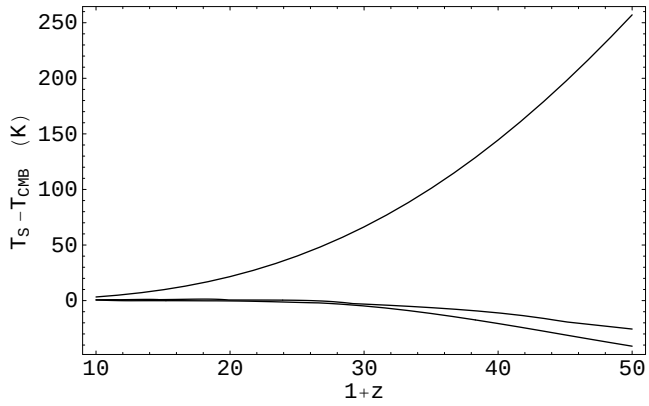

FIG. 9: Zoom in of fig. 8 at redshifts more accessible to 21 cm. The difference between the spin and CMB temperatures are shown for seed white noise power, from bottom to top, $M_H = 10^{-3}M_\odot,\ 1M_\odot,\ 10^3M_\odot$). The 10^{-3} curve is indistinguishable from the predictions of CDM (the short dashed line in fig. 7).

of the gas, the curves in figs. 8,9 should thus be interpreted as a lower bound on the heating effect. At $z < 20$ however, where the first tomographic experiments will operate, it may be difficult to distinguish these effects from heating by stars.

The white noise hierarchy generates a rising mean temperature but also a range of temperatures. Not all baryons are heated to the (continually rising) dark matter virial temperature as the hierarchy forms. Particularly if cooling is inefficient and stars do not form, some baryons remain in the minihalos in which they first collapsed, which have a lower virial temperature than those currently collapsing and shock heating. As a result, there is range of temperatures and densities contributing to 21 cm absorption or emission at high redshift: baryons which are heated to the virial temperature of newly formed dark matter halos in the hierarchy, as well as baryons which remain in the cooler minihalos. While the baryons in the minihalos are cooler, the density of baryons in the minihalos is much higher than in the heated, diffuse gas. Once they are formed, their kinetic and spin temperature remains low, while the CMB photon temperature continues to drop with redshift. As a result, these objects will result in less absorption of CMB photons at high redshift as compared to standard CDM, and eventually this weakened absorption will turn into emission, rather than absorption, of the 21 cm line. We summarize this situation in table I.

Another phenomenological feature in the tomographic signal worth mentioning is the angular white noise from inhomogeneous heating. The main new contribution to the signal we have been discussing assumes that the spatial density distribution on large scales is the same as standard CDM, and the departure from this comes about from the significant change in mean spin temperature of the diffuse HI gas. But an additional signal arises from the fact that the spin temperature itself has a white noise spatial component from the random heating, that can in principle dominate over the density perturbations on large scales. This effect adds yet more power to the tomography signal which is not calculated here.

$M_H\ (M_\odot)$	z_b	minihalo T_S (K)	z_{emit}
10^3	600	1500	600
1	50	90	30
10^{-3}	15	40	15
10^{-6}	15	40	15

TABLE I: For a given white noise power spectrum associated with mass M_h, the redshift at which baryons begin accreting on minihalos, z_b; the minihalo spin temperature, T_S; and the redshift, z_{emit}, at which the baryons accreted onto the minihalo begin emitting rather than absorbing the 21 cm line.

V. CONCLUSION

We have shown that the addition of white noise to the inflationary power spectrum can alter the history of structure formation and baryon collapse, and lead to modified 21 cm emission and absorption from gas at high redshift. The effect of the white noise is to seed early bottom-up hierarchical structure formation onto which baryons can collapse, leading to early heating of the baryons through accretion onto dark matter halos. This early heating leads to higher kinetic and spin temperatures, with departures from standard CDM at redshifts $z \gtrsim 30$ if the seed dark matter halo has mass $\gtrsim 1M_\odot$. At higher seed mass $\gtrsim 10M_\odot$ the additional white noise also leads to early star formation; although the observable effects of that are very model dependent, there are clearly

departures expected from ΛCDM. For $M_H < 1M_\odot$ the effects appear to be hard to detect since the halo temperature is cooler than the baryon temperature until the standard inflationary fluctuations begin their collapse.

The observation of such macroscopic astrophysical effects would hint at exotic microphysics in the dark sector. Standard thermal relics, such as WIMPs and axions, do not give rise to deviations from the inflationary power spectrum that are observable by these techniques. The most natural source for the extra small scale noise arises from other dark matter dynamics, such as a scalar field phase transition. The signatures discussed here complement effects of similar minihalo masses that might be observed in gravitational lensing and other lower-redshift effects [15].

Acknowledgments

We are grateful to N. Afshordi, M. Morales and E. Siegel for helpful comments. This work was supported in part by the U.S. Department of Energy under grant No. DE-FG02-95ER40896.

[1] D. N. Spergel et al. (2006), astro-ph/0603449.
[2] J. K. Adelman-McCarthy et al. (SDSS), Astrophys. J. Suppl. **162**, 38 (2006), astro-ph/0507711.
[3] S. Cole et al. (The 2dFGRS), Mon. Not. Roy. Astron. Soc. **362**, 505 (2005), astro-ph/0501174.
[4] P. McDonald, U. Seljak, S. Burles, D. J. Schlegel, D. H. Weinberg, R. Cen, D. Shih, J. Schaye, D. P. Schneider, N. A. Bahcall, et al., Astorphys. J. Supp. **163**, 80 (2006), astro-ph/0405013.
[5] A. Loeb and M. Zaldarriaga, Phys. Rev. **D71**, 103520 (2005), astro-ph/0504112.
[6] J. Diemand, B. Moore, and J. Stadel, Nature. **433**, 389 (2005), astro-ph/0501589.
[7] E. W. Kolb and I. I. Tkachev, Astrophys. J. **460**, L25 (1996), astro-ph/9510043.
[8] D. N. Spergel and P. J. Steinhardt, Phys. Rev. Lett. **84**, 3760 (2000), astro-ph/9909386.
[9] M. Kaplinghat, L. Knox, and M. S. Turner, Phys. Rev. Lett. **85**, 3335 (2000), astro-ph/0005210.
[10] J. L. Feng, A. Rajaraman, and F. Takayama, Phys. Rev. **D68**, 063504 (2003), hep-ph/0306024.
[11] L. E. Strigari, M. Kaplinghat, and J. S. Bullock (2006), astro-ph/0606281.
[12] K. Abazajian, G. M. Fuller, and M. Patel, Phys. Rev. **D64**, 023501 (2001), astro-ph/0101524.
[13] S. Dodelson and L. M. Widrow, Phys. Rev. Lett. **72**, 17 (1994), hep-ph/9303287.
[14] X.-D. Shi and G. M. Fuller, Phys. Rev. **D59**, 063006 (1999), astro-ph/9810075.
[15] K. M. Zurek, C. J. Hogan, and T. R. Quinn (2006), astro-ph/0607341.
[16] N. Afshordi, P. McDonald, and D. N. Spergel, Astrophys. J. **594**, L71 (2003), astro-ph/0302035.
[17] M. F. Morales, Astrophys. J. **619**, 678 (2005), astro-ph/0406662.
[18] M. F. Morales, J. D. Bowman, and J. N. Hewitt, Astrophys. J. **648**, 767 (2006), astro-ph/0510027.
[19] R. Barkana and A. Loeb, Phys. Rept. **349**, 125 (2001), astro-ph/0010468.
[20] S. Furlanetto, S. P. Oh, and F. Briggs, Phys. Rept. **433**, 181 (2006), astro-ph/0608032.
[21] X.-H. Fan, C. L. Carilli, and B. Keating, Ann. Rev. Astron. Astrophys. **44**, 415 (2006), astro-ph/0602375.
[22] C. J. Hogan and M. J. Rees, Phys. Lett. **B205**, 228 (1988).
[23] E. W. Kolb and I. I. Tkachev, Phys. Rev. Lett. **71**, 3051 (1993), hep-ph/9303313.
[24] A. Loeb and M. Zaldarriaga, Phys. Rev. Lett. **92**, 211301 (2004), astro-ph/0312134.